CO_2 激光作用下直流 TIG 电弧特性分析

张寰臻， 吴世凯， 肖荣诗
（北京工业大学 激光工程研究院，北京 100124）

张寰臻

摘 要：文中借助高速摄像和激光功率计等先进手段，研究了 CO_2 激光与直流 TIG 电弧垂直相互作用时激光对电弧特性的影响. 激光功率越高，电弧静特性曲线下移幅度越大，电弧电功率越低，而电弧总功率越高. 电弧电流越小、激光作用位置越靠近阴极，电弧电压下降幅度越大. 激光作用引起电弧体积膨胀主要发生在激光作用位置到阳极之间的区域. 结果表明，激光作用电弧后，电弧静特性曲线下移，体积膨胀，电弧电功率下降，而总功率增加.

关键词：钨极惰性气体保护焊； CO_2 激光； 电弧静特性； 电弧形态； 电弧功率
中图分类号：TN249 文献标识码：A 文章编号：0253－360X(2009)03－0097－04

0 序 言

始于 20 世纪 70 年代末的激光电弧复合焊接，是一种综合了激光与电弧各自特点的先进连接技术. 由于在提高焊接效率的同时，改善激光焊接的桥接性，降低间隙敏感度，目前已在造船、汽车及管道连接中显示出独特的优势. 在实际的应用中，通过改变激光与电弧能量的比率，可实现从单纯的激光焊到电弧焊的过渡，以适应不同的加工要求[1,2].

目前，国内外对激光电弧复合焊接的研究方兴未艾，主要集中在复合方法、布置方式、电弧电流、激光功率、焊接速度、激光离焦量、激光与电弧的相对位置等工艺参数对焊缝熔深、成形、过程稳定性及等离子体状态的影响等方面[3~5]，但是关于激光与电弧的相互作用机理研究涉及较少. Natio 等人[6] 在 YAG-TIG 复合焊接过程中，利用 CCD 采集小孔前沿一定角度的反射光线来计算电弧对激光的散射、折射情况，结果表明复合焊接时电弧对 YAG 激光的散射、折射、吸收都较小. Hu 等人[7] 使用功率计测量了 500 W Nd:YAG 激光垂直穿过 100 A 直流 TIG 电弧后能量损失仅为 0.7%，利用 Beer-Lambert 定律计算出电弧对 YAG 激光的吸收系数仅为 1.03×10^{-2} cm^{-1}. 陈彦宾等人[8,9] 采用激光烧蚀有机玻璃方法定性得出较低功率 CO_2 激光垂直穿过电弧时，电弧阴极区对激光吸收较弱，阳极区吸收较强；并在研究激光旁轴 TIG 电弧焊缝特征时观察到了激光支持的燃烧波，认为电弧的存在使得燃烧波的产生更加容易. Seyffarth[10] 归纳激光－电弧同轴复合的机理时指出，由于激光光束半径小，对电弧局部加热效率远大于电弧焦耳热，电弧中心通道温度及电流密度的提高，改变了电弧能量的状态分布.

文中借助激光功率计、高速摄像仪等手段，研究 CO_2 激光垂直作用时直流 TIG 电弧特性的变化规律.

1 试验方法

试验采用 Rofin DC035 Slab CO_2 激光器，光束模式为准 TEM00 模，经焦距 300 mm 的旋转抛物反射聚焦镜聚焦，聚焦光斑直径 0.27 mm. 弧焊电源为 Fronius TS5000 数字焊机. 试验装置如图 1 所示. 聚焦激光束垂直作用于直流 TIG 电弧，焦点位于电弧中心. 电弧电极为铈钨极，阴、阳极直径分别为 2.5，30 mm，电极间距为 6 mm. 电弧气氛为流量 15 L/min 的 Ar. Molectron 3sigma 功率计布置于电弧后方测量穿过电弧后的激光功率. 使用美国 PHOTRON Fastcam 1024R2 彩色高速摄像仪（拍摄频率 2 000 帧/s）观测电弧形态变化，并用电压计记录电弧电压.

收稿日期：2008－01－21
基金项目：北京市教委科技发展计划重点项目(KZ200710005003)；国家教育部新世纪优秀人才支持计划(NCET－04－0204)；北京工业大学 111 人才工程基金资助项目

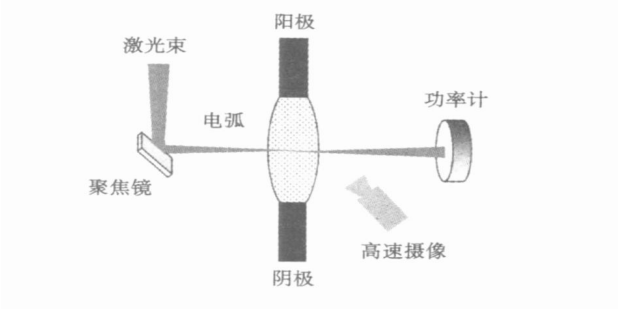

图 1 试验装置示意图

Fig. 1 Experimental setup

2 试验结果

2.1 电弧静特性

图 2 为激光作用于电弧中间位置时电弧静特性的变化. 可以看出, 激光的作用使电弧静特性曲线向下移动, 且电弧电流越小, 电压下降越明显; 激光功率越高, 电弧静特性曲线下移幅度越大.

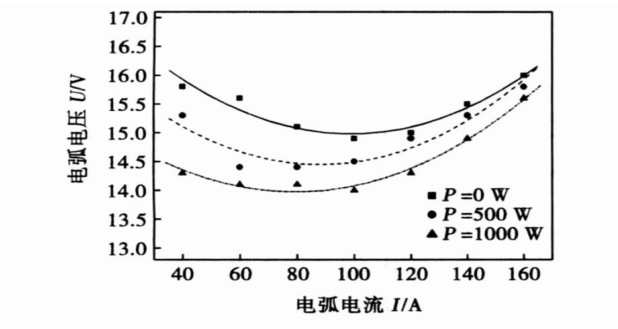

图 2 激光对电弧静特性的影响

Fig. 2 Effect of laser action on static characteristic of arc

图 3 为电弧电流 50 A 时, 激光作用于电弧不同位置电弧电压随激光功率变化曲线. 可以看出, 激光作用距离阴极较近时, 电压下降明显; 作用位置越远离阴极, 电压降低越少; 激光作用靠近阳极时, 电压几乎不变.

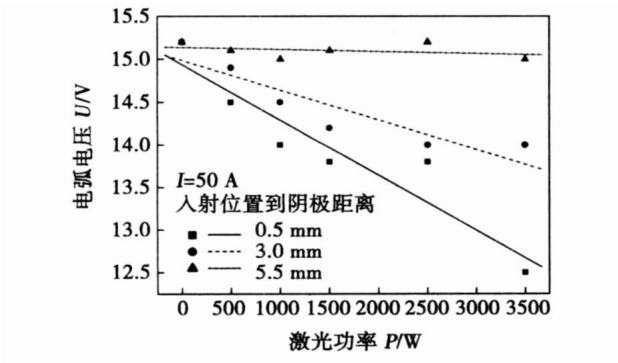

图 3 激光作用位置对电弧电压的影响

Fig. 3 Effect of laser-arc interaction position on arc voltage

2.2 电弧形态

图 4 为激光作用电弧不同位置时的电弧形态, 其中激光功率 500 W, 电弧电流 50 A. 从图中明显看出, 激光作用电弧后引起电弧体积膨胀, 且膨胀主要发生在激光作用位置到阳极之间, 当激光作用于阴极附近则引起整个电弧体积膨胀.

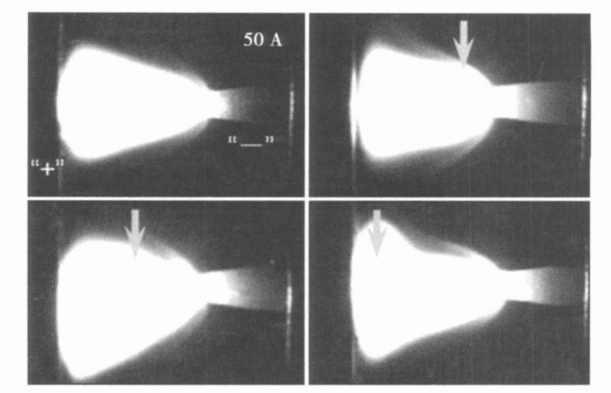

图 4 激光作用位置对电弧形态的影响(图中箭头指示为激光作用位置)

Fig. 4 Effect of laser-arc interaction position on arc configuration(arrow indicates incident laser)

2.3 电弧注入总功率

图 5 为电弧电流 50 A, 激光功率 500 W 时, 激光作用于电弧不同位置时电弧电功率及总功率的变化, 其中 $U_0 I_0$ 为电弧原始电功率. 可见, 激光作用电弧后, 注入电弧的电功率降低. 激光作用位置离阴极越近, 注入电弧的电功率越小. 但是, 电弧吸收部分激光能量而使电弧的总功率增加, 激光作用位置离阴极越远, 电弧电功率和总功率越高, 且总功率的增长幅度高于电功率的增长幅度, 这是由于吸收的

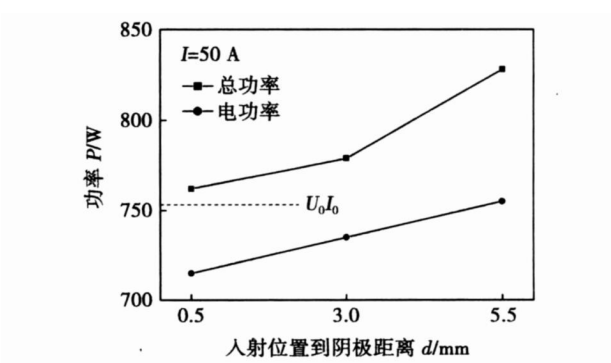

图 5 激光作用位置对电弧电功率及总功率影响

Fig. 5 Effects of laser-arc interaction position on electric power and total power of arc

激光能量增加的缘故. 图 6 为激光作用于电弧中间位置时激光功率对电弧总功率的影响. 激光功率越高，虽然电弧电压及电功率越低，但由于电弧对激光的吸收加强，电弧的总功率越高.

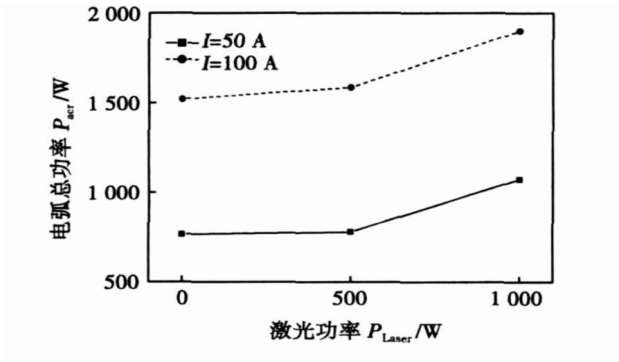

图 6　激光功率对电弧总功率的影响

Fig. 6　Effect of laser power on arc power

3　分析与讨论

激光作用电弧时，电弧等离子体通过逆韧致辐射吸收部分激光能量，表征电子能量的动力论二阶矩方程[11—13]可修正为

$$\frac{\partial}{\partial t}\left(\frac{3}{2}kn_eT\right)=\kappa\nabla^2T-\frac{5}{2}k\vec{\Gamma}_e\cdot\nabla T-S(T,n_i)+\vec{j}_e\cdot\vec{E}+K_\alpha(I_0e^{-K_\alpha z}) \quad (1)$$

式中：n_e 为电子密度；T 为等离子体温度；κ 为热导率；k 为波尔兹曼常数；$\vec{\Gamma}_e$ 为电子流（$\vec{j}_e=e\vec{\Gamma}_e$）；$j_e$ 为电流密度；E 为电场强度；K_α 为 IB 吸收系数；I_0 为激光初始功率密度；z 为激光在电弧中的传输距离；$S(T,n_i)=1.42\times10^{-34}Z^2n_i^2T^{1/2}$ (W/cm^{-3})[14] 为离子韧致辐射的功率密度，它与离子密度 n_i 及温度正比，其中 Z 为离子价数.

式(1) 右边五项分别为热传导、对流、辐射、电弧焦耳热及逆韧致辐射吸收的激光能量. 在热平衡条件下，单位时间注入单位体积电弧等离子体总能量与热传导、对流及辐射散失的能量相等，能量守恒方程为

$$\vec{j}_e\cdot\vec{E}+K_\alpha(I_0e^{-K_\alpha z})=-\kappa\nabla^2T+\frac{5}{2}k\vec{\Gamma}_e\cdot\nabla T+S(T,n_i) \quad (2)$$

由试验结果已知，激光作用电弧后，注入到电弧的总能量增加，从而使得电弧中心温度升高，促使电弧气氛的电离度和导电粒子数增加，因此电弧电阻率降低，静特性曲线下移. 电弧电流越小，原始电弧气氛的电离度越低，激光的作用引起电离度和导电粒子数增加的效果越明显，电弧电阻率和电压降低越显著. 激光功率越高，电弧吸收的激光能量和电弧总能量越高，电弧气氛的电离度和导电粒子数增加幅度越大，电弧静特性曲线下移幅度也就越大.

根据电弧的导电机制，在弧柱中，虽然同时存在离子和电子，但是由于两者质量相差很大，离子对电流的贡献仅为电子的 1/1000 左右，弧柱电流几乎为电子流[15]. 因此，当激光作用电弧时，电弧吸收的激光能量将主要通过电子流向阳极输运，亦即激光对电弧的影响主要发生在激光作用位置到阳极之间，这就是为什么激光作用引起电弧的膨胀主要发生在激光作用位置到阳极之间的原因.

在激光的作用下，电弧弧柱电压可表示为 $U=E'\times l'+E''\times l''$，其中 E'，E'' 分别为激光作用位置至阴极和阳极之间弧柱电场强度，l'，l'' 为对应的弧长. 激光作用位置距离阴极越近，激光的作用对电弧的影响区间越大，$E''\times l''$ 占总电压的比例越大，因此电弧电压降低越明显，输入的电功率越低.

激光作用位置离阴极越远，亦即离阳极越近，电弧总功率越高是由两方面的原因造成的. 其一，激光作用位置越靠近阳极，激光的作用对电弧的影响区间越小，电弧电压降低越少，注入的电功率越大；其二，电弧吸收激光能量的多少与激光在电弧中的传输长度有关. 激光作用位置越靠近阳极，电弧尺寸越大，激光在电弧中传输的距离越长，吸收的激光能量越多.

4　结　　论

(1) CO_2 激光作用直流 TIG 电弧时，电弧静特性曲线下移. 激光功率越大，电弧静特性曲线下移幅度越大.

(2) 电弧电流越小，激光的作用导致电弧电压下降幅度越大；激光作用位置越靠近阴极，电弧电压降低越明显.

(3) 激光作用使电弧的电功率降低，而总功率增加. 激光功率越高，电弧电功率越低，总功率越高.

(4) 激光作用使电弧体积膨胀，膨胀主要发生在激光作用位置到阳极之间的区域.

参考文献：

[1] Steen W M. Arc augmented laser processing of materials [J]. Journal of Applied Physics, 1980, 51(11): 5636—5641.

[2] Jasnau U, Hoffmann J, Seyffarth P. Nd: YAG-laser-GMA-hybrid

welding in shipbuilding and steel construction [J]. Robotic Welding, Intelligence and Automation, 2004, 299: 14—24.

[3] Natio Y, Katayama S, Matsunawa A. Keyhole behavior and liquid flow in molten pool during laser—Arc hybrid welding [C] // Osaka Japan Proceeding of SPIE, 2003, 4831: 357—362.

[4] Bagger C, Olsen F O. Review of laser hybrid welding [J]. Journal of Laser Applications, 2005, 17(1): 2—14.

[5] Ishide T, Tsubota S, Watanabe M. Latest MIG, TIG arc-YAG laser hybrid welding systems for various welding products [C] // Osaka Japan Proceeding of SPIE, 2003, 4831: 347—352.

[6] Naito Y, Mizutani M, Katayama S. Plasma/plume behavior during welding: welding phenomena in hybrid welding using YAG laser and TIG arc [J]. Welding International, 2006, 20(10): 777—784.

[7] Hu B, Ouden G D. Laser induced stabilization of the welding arc [J]. Science and Technology of Welding and Joining, 2005, 10(1): 76—80.

[8] 陈彦斌, 李俐群, 吴 林. 电弧对激光吸收与散焦的定量测量 [J]. 焊接学报, 2003, 24(3): 56—58.
Chen Yanbin, Li Liqun, Wu Lin. Measurement of laser absorption and defocusing by arc [J]. Transactions of the China Welding Institution, 2003, 24(3): 56—58.

[9] 陈彦斌, 陈 杰, 李俐群. 激光与电弧相互作用时的电弧形态及焊缝特征 [J]. 焊接学报, 2003, 24(1): 55—56.
Chen Yanbin, Chen Jie, Li Liqun. Properties of arc and weld in laser—TIG hybrid process [J]. Transactions of the China Welding Institution, 2003, 24(1): 55—56.

[10] Seyffarth P, Krivtsun I V. Laser-arc processes and their applications in welding and material treatment [M]. Great Britain, 2002.

[11] Lancaster J F. The physics of welding-2nd edition [M]. Great Britation, 1986.

[12] Wang Q, Economou D J, Donnelly V M. Simulation of a direct current microplasma discharge in helium at atmospheric pressure [J]. Journal of Applied Physics, 2006, 100: 023301—1—023301—10.

[13] Tix C, Gratzke U, Simon G. Absorption of the laser beam by the plasma in deep laser beam welding of metals [J]. Journal of Applied Physics, 1995, 78(11): 6448—6453.

[14] 克拉尔, 特里维尔 皮斯. 等离子体物理学原理 [M]. 郭书印, 黄 林, 邱孝明, 译. 北京: 原子能出版社, 1983.

[15] 安藤弘平, 长谷川光雄. 焊接电弧现象 [M]. 施雨湘, 译. 北京: 机械工业出版社, 1985.

作者简介: 张寰臻, 女, 1982 年出生, 硕士研究生. 主要从事激光—电弧相互作用研究. 发表论文 1 篇.

Email: huanwozhenzhen@gmail.com

posite bonds increases by 50% than that of the brazed bond without SiC particles. The increased strength is associated with the increase of the aluminum content and the quantity of reinforcement particles in the bond metal.

Key words: aluminum matrix composites; ultrasonically aided brazing; shear strength; microstructure; formation of composite joint

Model of forces on pin tool and its application ZHOU Li, LIU Huijie, LIU Peng (National Key Laboratory of Advanced Welding Production Technology, Harbin Institute of Technology, Harbin 150001, China). p93—96

Abstract: A model of forces on pin tool in the plunge stage and the steady welding stage during the friction stir welding (FSW) process is established and verified by comparison with experimental data. It indicates that pin root is the weakest portion of the pin tool in either the plunge stage or the steady welding stage. Pin tool can fail from the root if improper design is adopted, so the model is applied to guide design of tools for FSW of Ti-6Al-4V. The results show that proper tool design is vital to FSW for Ti-6Al-4V. Sound welds could be obtained under appropriate parameters.

Key words: friction stir welding; pin tool; model of force; Ti-6Al-4V

Characteristics of DC TIG arc with the action of a vertically incident CO_2 laser beam ZHANG Huanzhen, WU Shikai, XIAO Rongshi (Institute of Laser Engineering, Beijing University of Technology, Beijing 100022, China). p97—100

Abstract: Laser-arc hybrid welding is one of the advanced joining techniques. By using instruments such as a high-speed camera and a laser power meter, the effects of a vertically incident CO_2 laser beam on characteristics of a DC tungsten inter-gas arc are investigated. Results demonstrate that the laser-arc interaction causes the curve of arc static characteristic to shift downwards, the arc column to expand, the electric power to decease and the total arc power increase. With the increase of the laser power, the downward shift of the static characteristic curve increases, but the total arc power increases. The lower the arc current is and the nearer the laser beam locates to the cathode, the more the arc voltage decreases, which the expansion of the arc column mainly occurs in the range between the laser beam location and the anode.

Key words: tungsten inter-gas; CO_2 laser; static characteristic of arc; arc configuration; arc power

Fatigue analysis of welded joints by method of structural stress WU Qi, QIU Huiqing, WANG Weisheng (Department of Mechanical Engineering, Tongji University, Shanghai 201804, China). p101—105

Abstract: Based on the structural stress method, some data of the fatigue strength of 16Mn, which include non-carrying-load fillet cruciform joints, carrying-load fillet cruciform joints and welded joints with longitudinal fillet welded gusset, are analyzed. The discrete structural stress formula which suits for finite element method are deduced, structural stress concentration factors for joints are obtained, and structural S-N curves for these joints are provided. The approach shows the good mesh-size insensitive characteristics. Compared with the nominal stress method, the dispersity of experimental data evaluated by structural stress method is reduced.

Key words: welded joints; fatigue assessment; structural stress

Spectra analysis and temperature measure of plasmas in YAG-MIG hybrid welding of 5A90 GUO Li[1], DUAN Aiqin[2], YU Yousheng[1] (1. School of Material Science and Engineering, Wuhan University of Technology, Wuhan 430023, China; 2. National Key Laboratory of High Energy Density Beam Processing Technology, Beijing Aeronautic Manufacturing Technology Research Institute, Beijing 100024, China). p106—108

Abstract: The spectra of vapor/plasmas were acquired by spectrometer during YAG-MIG hybrid welding of 5A90 Al-Li alloys in our research. The temperature values of the vapor/plasmas were calculated by the methods of relative intensity. The effects of arc current and heat input on the temperature of the vapor/plasmas were discussed. The results show that the spectra of hybrid welding in the range of 350—850 nm is mainly argon ion spectra line accompanied with a few Mg and Li ion. An average temperature under a set of processing parameters is 6554 K; compared to YAG welding, the value has an increase of 1200 K; however, it is near to the average temperature of MIG welding.

Key words: YAG-MIG hybrid welding; metal vapor/plasmas; spectrum

3-D numerical simulation of welding spherical valve core DING Hui, LEI Junxiang, ZHU Hanhua, LI Xinran (University of Shanghai for Science and Technology, Shanghai 200093, China). p109—112

Abstract: Welding is the key course in manufacturing the spherical valve core through steel tube's necking, assembling, welding and grinding. Because the necked workpiece is under stress before welding and is to be prepared for grinding after welding, how to choose sound welding parameters so as to control residual stress with the precondition of excellent weld quality becomes the focus of this paper. A series of numerical simulations which show the real-time dynamic changes under different welding parameters for necked workpiece are demonstrated, and the optimization parameters are obtained through comparing the welding size and residual stress after welding. Analysis and illustrations on the accumulated results show that the residual stress after welding is overlapped in the former procedures.

Key words: spherical valve core; necking; numerical simulation; parameter optimization